LAWRENCE
LIVERMORE
NATIONAL
LABORATORY

LLNL-JRNL-434371

A Complete Detonator, Booster and Main Charge Study of LX-07/PBX 9502

P. Clark Souers, Robert L. Druce, Franklin Roeske, Jr., Peter Vitello, Chadd May

June 8, 2010

Propellants, Explosives, Pyrotechnics

Disclaimer

A Complete Detonator, Booster and Main Charge Study of LX-07/PBX 9502

P. Clark Souers, Robert L. Druce, Franklin Roeske, Jr., Peter Vitello and Chadd May
Enegetic Materials Center
Lawrence Livermore National Laboratory, Livermore, CA 94550

Abstract. A complete study of an exploding bridge wire detonator, an LX-07 hemispherical booster and a PBX 9502 outer shell are described. Breakout times from all three are listed in terms of first impact on the booster, ie. code times. Lucite windows are also used to obtain particle velocities at the edges of each explosive, and these are converted into explosive pressures. The key to modeling is the use of the profile of the aluminum detonator can as it impacts the booster, ie., we need to know the curvature of end of the booster can. Modeling even with coarse zoning shows that 1) using reactive flow in the booster is better than programmed burn, 2) creating the flyer curvature helps and 3) creating the time difference of flyer impact helps even more.

Keywords: detonator, booster, breakout time, spike pressure, Fabry-Perot interferometry

Druce. et. al. previously described a study of breakout times from a TATB booster [1]. Also included were Lucite pressures derived from particle velocity measurements in window materials placed at various angles on the booster outer radius. The booster breakout times zeroed to the leading edge were taken as the main output. The relative importance of adding the window pressures in modeling was not considered. Since then, the desire has increased to push modeling back all the way to the detonator. This study uniquely combines data from a detonator, booster and main charge and includes both breakout times and pressures.

1. Experiment

The schematic of the geometry is shown in Figure 1. The booster is a hemisphere of 1.85 g/cc LX-07 of outer radius 15 mm. The detonator is recessed in a cavity at the back of the booster. The cavity has a radius of 3.85 mm and a depth of 1.27 mm, so that the distance from the detonator end to the LX-07 outer surface along the axis of rotation is 13.73 mm. The main charge outside is 1.89 g/cc PBX 9502 with an outer radius of 28.185 mm so that the thickness is 13.185 mm. The axis of rotation is always 0^{o}. The temperatures are ambient, cold (-54^{o}C) and hot (76.6^{o}C).

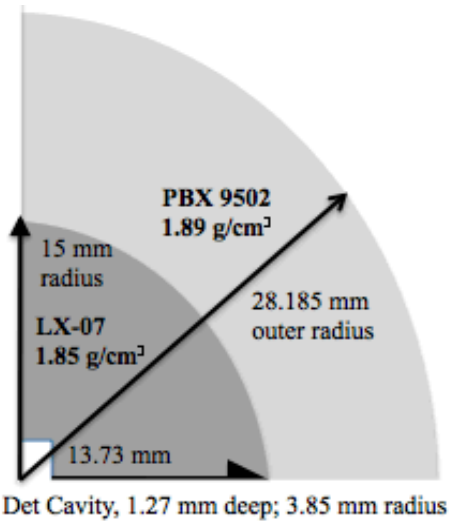

Figure 1. Schematic of the booster and main charge system.

The detonator is a cylindrical, exploding bridgewire detonator (EBW) inside an aluminum can. All times presented here are in code times, ie., referenced to the on-axis first breakout of the aluminum end of the detonator. The code times are more useful for modeling, where we expect that a simulated plate collision at time zero will be programmed. The time differences from bridge-burst time to detonator code time are 0.69, 0.74 and 0.69 μs for ambient, cold and hot.

A streak camera was used to measure the breakout profile of the detonator. This data in units of code time, are shown in Figure 2 with estimated standard deviations. At each temperature, there were about 7 or 8 shots with two right angle directions. The breakout looks the same at all three temperatures. The on-axis position at zero is the definition of code time. All the breakout data may be well summarized by the fit

$$t = 0.0158R^2, \qquad (1)$$

where t is the code time in μs and R is the radius in mm. The maximum radius is 3.82 mm.

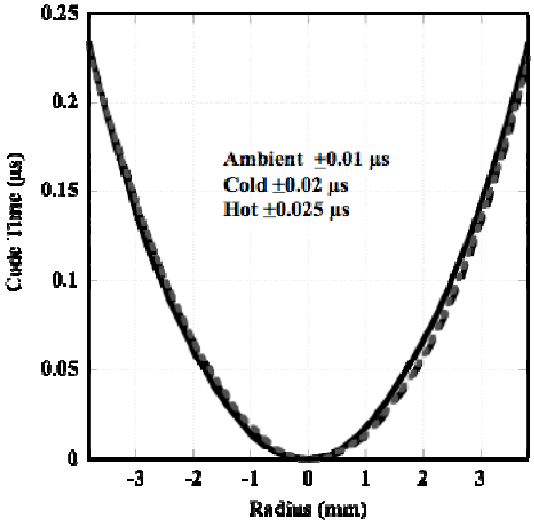

Figure 2. Averaged streak camera data from the front of the aluminum detonator can. The top solid line is ambient. The on-axis zero time is the start of code time.

Another detonator result is a Fabry-Perot interferometry measurement, using a lithium fluoride window, which is shown in Figure 3. The velocity has been divided by 1.28 to correct for the refractive index, so the measured maximum of 2.02 mm/µs drops to 1.58 mm/µs. The peak velocity in the LiF window shot may be converted to a LiF pressure, P_m, by way of

$$P_m = \rho_m \left(C_m + S_m \frac{u_m}{1.28} \right) \frac{u_m}{1.28}, \qquad (2)$$

where ρ_m is the LiF density of 2.638 g/cc, C_m and S_m are the LiF U_s-u_p coefficients (5.15 mm/µs and 1.35), and u_m is the measured particle velocity. The pressure attained in the window is 30.3 GPa. Using the impedance calculation, we find that 30 GPa is associated with 3 mm/µs for the aluminum end of the detonator can. As shown in Figure 3, the spike on the direct can measurements varies from 2.2 to 3.7 mm/µs, which is in general agreement.

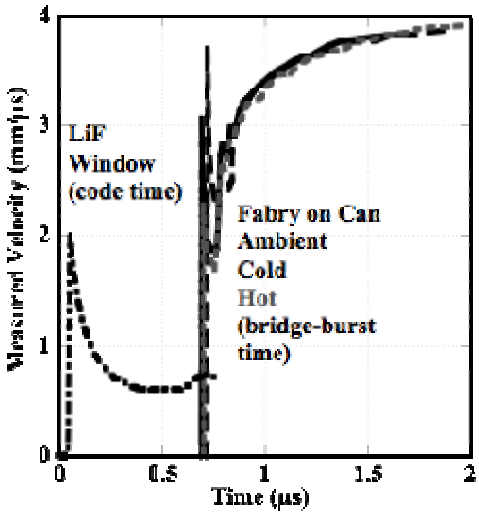

Figure 3. Fabry-Perot data taken on the detonator. Two times scales are used to separate the results. The LiF window data is to the left and the direct velocity of the aluminum can is to the right.

For the LX-07 booster, the breakout time data is shown in Figure 4, where three shots at each temperature have been combined. The leading edges of the breakout do not occur on-axis but at about 65^{o} for ambient and hot and at about 58^{o} for cold. The PMMA maximum velocity times agree with the streak camera for ambient and hot but are 4-5% higher when cold. The last seems a large difference, and we are not sure of the reason.

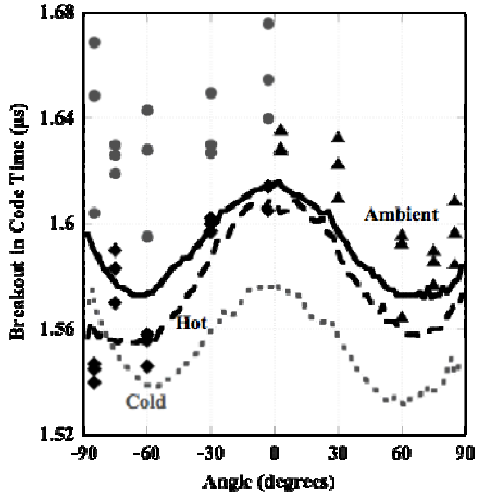

Figure 4. Combined booster streak breakout with maximum Fabry-Perot times. The data is ambient: solid line and triangles, cold: gray dotted line and circles, and hot: dashed lines and diamonds. The cold data shows a significant difference.

For the PBX 9502 outer layer, Figure 5 shows the streak breakout and Fabry-Perot maximum velocity times at all three temperatures, with PMMA again being used. The Fabry-Perot times agree at all temperatures with the streak times. The fastest part of the break-out is at about 65^{o} at ambient and hot and at 55^{o} cold- the same as occurred with the booster.

Next, we consider the maximum velocity measured by the Fabry-Perot interferometry. This is measured from a thin aluminum foil between the explosive and the PMMA. The pressure is calculated using

$$P_{x1} = \rho_{x1}\{C_{x1} + S_{x1}u_{x1}\}u_{x1} \qquad (3)$$

where ρ_m is the PMMA density (1.186 g/cc) and C_m and S_m are the U_s-u_p coefficients (2.57 mm/μs and 1.54). There is no refractive index correction to the PMMA. In the next section, we describe the conversion from the PMMA pressure to the explosive pressure, which is the desired output.

The Fabry data for the boosters is contained in Table 1. The final explosive pressures at the outer radius of the LX-07 boosters are shown in Figure 6. The estimated precision is $\pm$2 GPa ambient and cold and $\pm$1 GPa hot. This scatter comes from the lack of resolution in the time allotted to the velocity maximum at the jumpoff, whereas the entire curve has been taken for a full microsecond. In our opinion, the three temperatures show the same result and we have placed a single line through the data.

The Fabry-Perot data for the PBX 9502 main charge are contained in Table 2. The plotted results are shown in Figure 7. The scatter is $\pm$2 GPa for the ambient and hot, and probably more for the cold. A constant 35 GPa line is used to average all ambient and hot data, but the cold data is definitely plunging at large angles. We also note that virgin PBX 9502 was used for shots 554, 555, 557, 576 and 577 and recycled material for 556, 579 and 580, and there is no apparent difference.

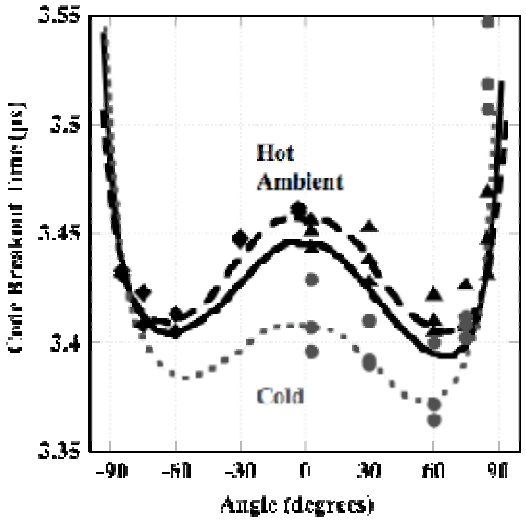

Figure 5. Breakout and maximum pressure times for all PBX 9502 samples. The data is ambient: solid line and triangles, cold: gray dotted line and circles, and hot: dashed lines and diamonds.

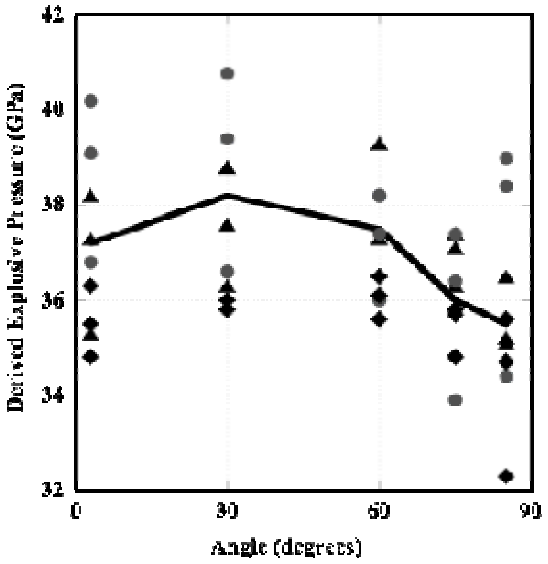

Figure 6. Pressures at the LX-07 booster outer edge as determined in a two-step process from measured Fabry-Perot velocities. The points are ambient triangles, cold gray circles and hot diamonds. All the data is averaged.

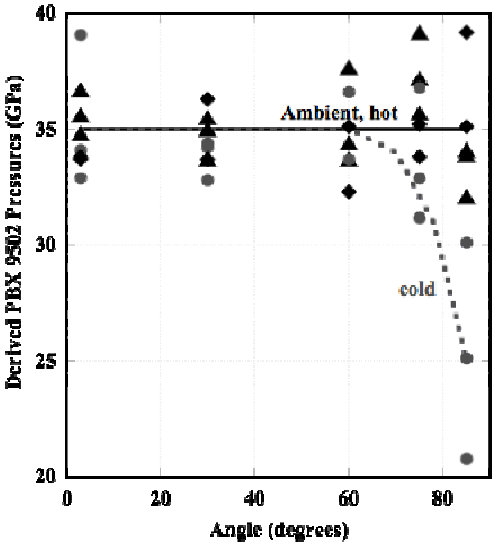

Figure 7. Pressures at the PBX 9502 shell outer edge as determined in a two-step process from measured Fabry-Perot velocities. The points are ambient triangles, cold gray circles and hot diamonds.

2 Pressure in an Explosive hitting a Optical Window

We have obtained peak velocities from windows, which are converted into window material pressures. But, we really want to know the corresponding pressure in the explosive. We turn to a 50 year-old equation derived for jump-off velocities of metal plates being pushed by the explosive [2-4]. If the window has a higher impedance, we get a higher pressure in the window, P_m, than the explosive, P, with a reshock pressure, P_r, so that

$$P_m = P + P_r = P + \rho_r U_r (u_p - u_m) \,, \tag{4}$$

where ρ_r is the reflected shock density, U_r the reflected shock wave velocity, and u_p and u_m are the explosive and metal particle velocities. The pressure being calculated is the maximum one, at the top of the spike, where the resolution of the spike is undefined. Then, the "acoustic approximation" says that

$$\rho_r U_r = \frac{4\rho_o}{3}\frac{3U_m}{4} \approx \rho_o U_m \tag{5}$$

where ρ_o is the initial density of the explosive, so that Eq. (5) imperfectly relates us to conditions we know about. The 4/3 comes from the approximate density at C-J and the ¾ assumes the speed of sound also at C-J. This assumption seems to work if the two materials have similar impedances. We now use the momentum conservation equations for each pressure for the explosive and window at the collision interface. Combining these equations, we get

$$P \approx \left(\rho_o U_s + \rho_m U_m\right)\frac{u_m}{2}. \tag{6}$$

Now, u_m is the particle velocity of the explosive-window interface that was just hit, which is the velocity we measure with the laser. This is twice as large as the velocity we would measure if air had been there instead of crystal. Eq. (6) works regardless of relative impedances. If the window has a lower impedance than the explosive, we have $P_m < P; u_m > u_p$; if the window has a higher impedance $P_m > P; u_m < u_p$.

Eq. (6) would be fine with a cylinder at steady state where we also measured the detonation velocity. But in a hemisphere, we don't know what it is. We can use the JWL-adjusting relation [5,6]

$$\frac{P}{P^o} = \left(\frac{U_s}{D}\right)^2 \tag{7}$$

where P and U_s are the maximum pressure and detonation velocity in the experiment and P^o and D are the same at infinite radius. We solve for U_s and substitute into Eq. (6) to get

$$P - \left[\frac{\rho_o u_m D}{2(P^o)^{1/2}}\right]P^{1/2} - \frac{\rho_m U_m u_m}{2} = 0. \tag{8}$$

The solution to the quadratic equation is

$$P = \left\{\left[\frac{\rho_o u_m D}{4(P^o)^{1/2}}\right] + \frac{1}{2}\left(\left[\frac{\rho_o u_m D}{2(P^o)^{1/2}}\right]^2 + 2\rho_m U_m u_m\right)^{1/2}\right\}^2 = 0. \tag{9}$$

We now have an equation but we have to calibrate P^o, which will be some measure of the spike. A guess might be 1.4 times the C-J pressure as determined from a thermochemical code. Because it will go into a code, it may be best to calibrate a cylinder at the desired zoning in the code and to correct all C-J

pressures using the extrapolated value of D. For our model at 4 zones/mm, we use 47 GPa for LX-07 and 37.7 GPa for PBX 9502.

The reactive flow model to be used needs to be calibrated at the zoning that the final problem will be run at. The calibration can be done using the detonation velocities of the small cylinder and the 1-inch cylinder as listed below for LX-17 and PBX 9502 at ambient. The peak pressure is measured for each cylinder and extrapolated back to infinite radius using an inverse radius plot.

3 Modeling

The main calculational tool is a 2-D ALE hydrocode, which is descended from CALE. In calculations, Lagrange zoning is used initially to ensure that the surfaces where measurement occurs have not had mass flow away from them and are well defined. To void zone tangling, Eulerian relaxation is applied away from the surfaces of measurement at later times.

Three kinds of models were created for square zones at 2 and 4 zones/mm, which are typical of today's large simulations and which is too coarse in every case to be accurate. All three models used reactive flow JWL++ [7] for the PBX 9502 outer shell, where 4 zones/mm is considered the edge of convergence. The models were as follows.

1. Programmed burn LX-07 using line detonation with Eq. (1) curvature set at the backside of the booster, so that the detonator cavity is empty. The detonator consists of individual detonators set inside each zone along the defined curve. This gives curvature but no time difference for impact. It is, at least, a step beyond a point detonation.

2. Fill the detonator cavity with explosive and create a programmed burn line with the Eq. (1) actual spatial curvature and detonation set zone-by-zone. This gives the programmed burn a 1.27 mm run before hitting the booster, which is modeled with reactive flow JWL++ with the power of the pressure b = 2, and the rate constant G = 1000 $(\mu s \cdot Mb)^{-1}$. The zoning is far too coarse for such an ideal explosive, but this creates a pressure spike and some curvature.

3. Creation of an aluminum flyer with the curvature of Eq. (1) set so that the leading point on the axis touches the back-side of the booster. The aluminum flyer thickness is taken to be 0.18 mm, which is the mean wall thickness in a RISI detonator. The flyer is given a velocity of 3 mm/μs, based on impedance calculations. The booster is again done coarsely with JWL++.

Figure 8 shows the breakout times for the booster with the leading point set to zero. All the models, done at 4 zones/mm, show the leading edge at 65-80^{o}, whereas a point detonation would have placed it on the axis. Even #1 with some curvature to the detonator is better than a point initiation. The #2 run adds in a time delay between the center and top of the flyer, which improves the results. The #3 with an actual curved detonator that takes time to complete its impact is the best. Using even a too-coarse reactive flow model for the booster is better than programmed burn. All runs needed the minimum 4 zones/mm, even with programmed burn, which is indeed zone-dependent. Going to 2 zones/mm is too coarse for good results.

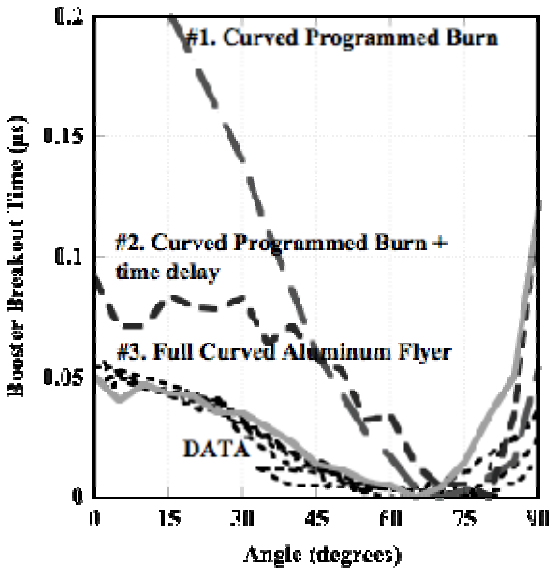

Figure 8. Calculated booster breakout times at 4 zones/mm. The data is shown by the dotted lines at the bottom.

4 Summary

A complete set of data representing detonator, booster and main charge is given here, with the essential data being the breakout time. The new data is the peak pressure measured by Fabry-Perot interferometry, but this appears to have an accuracy of ±2-3 GPa and results in the scatter seen in Figures 6 and 7. The measured traces were often as long as 1 μs, whereas high resolution over the first 0.1 μs in the optical material is what is really needed to get the true peak.

The modeling shows that a desire to include the booster with the main charge quickly leads back to the detonator as well. Using point charge initiation no longer works and the initiation front should be modeled with curvature and time delay. Modeling the actual slapper is really the way to go if enough zones are

available. At least 4 zones/mm are needed because even programmed burn is zone-dependent. Using reactive flow is better than programmed burn for the booster breakout times, even if the zoning is too coarse. Reactive flow becomes essential if the measured pressure peaks are considered, because programmed burn has no spike at all. If the main charge has any kind of initiation threshold, then a programmed burn booster cannot properly start the next stage.

Table 1. Times and Fabry-Perot velocities and pressures for the LX-07 booster.

		Code	Peak	Peak Pressure				Code	Peak	Peak Pressure	
shot	Angle	time	velocity	PMMA	Expl.	shot	Angle	time	velocity	PMMA	Expl.
#	(deg)	(μs)	(mm/μs)	P_m (GPa)	P (GPa)	#	(deg)	(μs)	(mm/μs)	P_m (GPa)	P (GPa)
ambient						529	60	1.628	3.162	27.9	36.0
518	3	1.636	3.129	27.4	35.3	527	75	1.626	3.059	26.4	33.9
525	3	1.628	3.264	29.4	38.2	528	75	1.630	3.179	28.1	36.4
526	3	1.629	3.222	28.8	37.3	529	75	1.619	3.228	28.9	37.4
518	30	1.633	3.240	29.1	37.6	527	85	1.604	3.081	26.7	34.4
525	30	1.623	3.293	29.8	38.8	528	85	1.669	3.303	30.0	39.0
526	30	1.610	3.174	28.1	36.3	529	85	1.649	3.278	29.6	38.4
518	60	1.596	3.320	30.3	39.3	hot					
525	60	1.565	3.225	28.8	37.3	530	3	1.614	3.136	27.5	35.5
526	75	1.590	3.214	28.7	37.1	531	3	1.614	3.103	27.0	34.8
525	75	1.586	3.230	28.9	37.4	532	3	1.605	3.176	28.1	36.3
526	75	1.577	3.176	28.1	36.3	530	30	1.600	3.150	27.7	35.8
518	85	1.609	3.116	27.2	35.1	531	30	1.602	3.160	27.9	36.0
525	85	1.585	3.122	27.3	35.2	532	30	1.597	3.159	27.9	36.0
526	85	1.597	3.183	28.2	36.5	530	60	1.556	3.165	27.9	36.1
cold						531	60	1.558	3.188	28.3	36.5
527	3	1.640	3.200	28.5	36.8	532	60	1.546	3.144	27.6	35.6
528	3	1.676	3.362	30.9	40.2	530	75	1.570	3.147	27.7	35.7
529	3	1.655	3.309	30.1	39.1	531	75	1.590	3.104	27.1	34.8
527	30	1.627	3.192	28.3	36.6	532	75	1.583	3.152	27.8	35.8
528	30	1.650	3.321	30.3	39.4	530	85	1.547	2.978	25.3	32.3
529	30	1.630	3.385	31.2	40.8	531	85	1.545	3.097	27.0	34.7
527	60	1.595	3.229	28.9	37.4	532	85	1.540	3.141	27.6	35.6
528	60	1.643	3.267	29.5	38.2						

Table 2. Times and Fabry-Perot velocities and pressures for the PBX 9502 outer shell.

		Code	Peak	Peak Pressure				Code	Peak	Peak Pressure	
shot	Angle	time	velocity	PMMA	Expl.	shot	Angle	time	velocity	PMMA	Expl.
#	(deg)	(μs)	(mm/μs)	P_m (GPa)	P (GPa)	#	(deg)	(μs)	(mm/μs)	P_m (GPa)	P (GPa)
ambient						577	30	3.390	3.054	26.3	34.4
554	3	3.457	3.165	27.9	36.7	557	60	3.400	3.160	27.9	36.6
555	3	3.452	3.112	27.2	35.6	576	60	3.372	3.020	25.9	33.7
556	3	3.444	3.071	26.6	34.8	577	60	3.365	3.020	25.9	33.7
554	30	3.454	3.107	27.1	35.5	557	75	3.412	2.978	25.3	32.9
555	30	3.439	3.083	26.8	35.0	576	75	3.402	2.895	24.1	31.2
556	30	3.429	3.019	25.9	33.7	577	75	3.408	3.171	28.0	36.8
554	60	3.423	3.055	26.4	34.4	557	85	3.507	2.563	19.8	25.1
555	60	3.411	3.020	25.9	33.7	576	85	3.519	2.300	16.7	20.8
556	60	3.406	3.214	28.7	37.7	577	85	3.547	2.837	23.3	30.1
554	75	3.427	3.283	29.7	39.2	hot					
555	75	3.410	3.190	28.3	37.2	579	3	3.462	3.026	25.9	33.8
556	75	3.408	3.117	27.2	35.7	580	3	3.460	3.018	25.8	33.7
554	85	3.470	3.030	26.0	33.9	579	30	3.448	3.020	25.9	33.7
555	85	3.448	2.939	24.7	32.1	580	30	3.447	3.144	27.6	36.3
556	85	3.432	3.038	26.1	34.1	579	60	3.405	2.949	24.9	32.3
cold						580	60	3.413	3.088	26.8	35.1
557	3	3.429	3.279	29.6	39.1	579	75	3.408	3.025	25.9	33.8
576	3	3.407	3.037	26.1	34.1	580	75	3.423	3.094	26.9	35.2
577	3	3.396	2.981	25.3	32.9	579	85	3.433	3.283	29.7	39.2
557	30	3.410	2.973	25.2	32.8	580	85	3.431	3.090	26.9	35.1
576	30	3.392	3.046	26.2	34.2						

Acknowledgments

This work performed under the auspices of the U.S. Department of Energy by Lawrence Livermore National Laboratory under Contract DE-AC52-07NA27344

References

1 R. L. Druce, P. C. Souers, C. Chow, F. Roeske, Jr., P. Vitello and C. Hrousis, "Detonation in TATB Hemispheres," *Propellants, Explosives, Pyrotechnics*, **2005**, *30* [2], 95-100.

2 J. M. Walsh and R. H. Christian, "Equation of State of Metals from Shock Wave Measurements," *Phys. Rev.,* **1955***, 97*, 1544-1556.

3 R. E. Duff and E. Houston, "Measurement of the Chapman-Jouguet Pressure and Reaction Zone Length in a Detonating High Explosive," *J. Chem. Phys.,* **1955***, 23*, 1268-1273.

4 W. E. Deal, "Measurement of Chapman-Jouguet Pressure for Explosives," *J. Chem. Phys.,* **1957***, 27*, 796-800.

5 P. C. Souers, S. Anderson, E. McGuire, M. J. Murphy and P. Vitello, "Reactive Flow and the Size Effect," *Propellants, Explosives, Pyrotechnics,* **2001***, 25*, 26-32.

6 P. Vitello, R. Garza, A. Hernandez and P. C. Souers, "The Energy Diameter Effect," *15th APS Topical Conference on Shock Compression of Condensed Matter*, Kohala Coast, HI, **2007**, June 23-29, pp. 877-880.

7 P. Clark Souers, Steve Anderson, Estella McGuire and Peter Vitello, "JWL++: A Simple Reactive Flow Code Package for Detonation," *Propellants, Explosives, Pyrotechnics,* **2000***, 25*, 54-58.